The Equatorial Waves of Balanced Models

PETER R. GENT AND JAMES C. MCWILLIAMS

National Center for Atmospheric Research,[1] Boulder, CO 80307

(Manuscript received 21 December 1982, in final form 6 April 1983)

ABSTRACT

An analysis is made of the linear waves of the Balance Equations and the global Balance Equations on an equatorial β-plane. We consider both finite and infinite meridional domains and show the effect of different choices of boundary conditions in a finite domain. The infinite domain is similar to a complete spherical domain, a problem studied by Moura. We find analogies to several of his results: for example, the Balance Equations have no eastward traveling waves, whereas the global Balance Equations do. We also make an extensive study of the long-wave limit, which is relevant for ocean domains whose width greatly exceeds the Rossby radius of deformation. This limit is singular for many of the wave solutions. In general, however, the balanced models provide reasonably good approximations to the low-frequency waves of the primitive equations. The global Balance Equations do have high-frequency waves, but they are very different from those of the primitive equations.

1. Introduction

In McWilliams and Gent (1980) we made a survey of models intermediate in complexity between the Primitive Equations (PE) and quasi-geostrophy. In Gent and McWilliams (1982) we found that the Balance Equations (BE) are a very good approximation to the PE for the wave-triad equations of Lorenz. This spurred us to further work on balanced models: consistent initial boundary value problems were formulated in Gent and McWilliams (1983a), and regimes of validity were discussed in Gent and McWilliams (1983b). All balanced models have a regime of validity that applies to a midlatitude situation in which the Coriolis frequency is approximated as a constant plus a function of the meridional coordinate. In an equatorial situation, when the above constant is set to zero, the BE are also a formally valid approximation to the PE in the long wave limit when the frequency and zonal wavenumber are both small. Also, the global Balance Equations (gBE), which include all the linear terms of the divergence equation and make no approximations in the horizontal component of the Coriolis force, have validity in very large or global domains in which the Coriolis frequency has order one changes. Given these formal regimes of validity, it would seem natural to use the BE and gBE in domains which span the equator. One aspect of model performance at the equator, which can be assessed fairly completely, is its linear wave response; thus the questions we ask in this paper are what are the linear equatorial waves of these two models, and how do they compare with those of the PE? The linear waves of the gBE are also those of the global Linear Balance Equations, and the waves of the BE are those of the Linear Balance Equations and the global Quasi-geostrophic model. All of these models are defined and discussed in Gent and McWilliams (1983a).

The equatorial waves of the PE in an infinite meridional domain are discussed in such works as Matsuno (1966), Holton (1969), and Moore and Philander (1977). The last paper is concerned with an oceanic situation with a finite zonal domain, and the waves in a bounded domain are considered, for example, in Cane and Sarachik (1979). The PE waves on an infinite equatorial β-plane are analogous to the waves of the Laplace Tidal Equations over a sphere. These waves have been comprehensively studied (e.g., see Lindzen, 1966; Longuet-Higgins, 1968). Moura (1976) studied the linear BE and gBE models over a sphere,[2] and so our infinite domain solutions should be analogous to his. Indeed they are, but we extend the analysis to a much more comprehensive study of the long-wave limit which is important when the ocean width greatly exceeds the deformation radius. This limit is singular for all waves in a meridionally infinite domain, and for those waves that have zonal velocity symmetric about the equator in a meridionally finite domain. There are several types of singularity which are discussed below. In a finite domain the waves with zonal velocity antisymmetric about

[1] The National Center for Atmospheric Research is sponsored by the National Science Foundation.

[2] Moura (1976) calls the gBE the "modified balance equations."

the equator are regular in the long wave limit. The analysis in a finite domain is new, and we show that the choice among the alternative boundary conditions defined in Gent and McWilliams (1983a) does mildly influence the linear waves of balanced models.

In the next section we derive the equations for the waves of balanced models, and discuss the methods used to solve them. Section 3 presents some general analytic results and some particular asymptotic analyses. The PE dispersion relation is briefly presented in Section 4. In Sections 5 and 6 we present numerical results for both finite and infinite domains for the BE and gBE, respectively. We summarize our results in Section 7, and Appendix A contains a detailed analysis of the long wave limit.

2. Equations and methods

a. Equations

We assume that large-scale atmospheric or oceanic flow is adiabatic, inviscid, Boussinesq and hydrostatic. The horizontal velocity can be decomposed into rotational and divergent components by

$$\mathbf{u} = \mathbf{e}_z \times \nabla\psi + \nabla\chi, \tag{1}$$

where $\mathbf{e}_z$ is a unit vertical vector. Then the BE, linearized about a stratified state of rest, are (see Gent and McWilliams, 1983a)

$$\textit{Vorticity} \qquad \nabla^2\psi_t + J(\psi, f) + \nabla\cdot(f\nabla\chi) = 0, \tag{2}$$

$$\textit{Divergence} \qquad \nabla\cdot(f\nabla\psi) = \nabla^2\phi, \tag{3}$$

$$\textit{Hydrostatic} \qquad \phi_z = \frac{g\theta}{\theta_0}, \tag{4}$$

$$\textit{Continuity} \qquad \nabla^2\chi + w_z = 0, \tag{5}$$

$$\textit{Heat} \qquad \theta_t + N^2 w = 0, \tag{6}$$

where J is the usual horizontal Jacobian operator. For the atmosphere ϕ, θ, and z are the geopotential, potential temperature, and a modified pressure coordinate, while for the ocean they are pressure divided by a reference density, minus the potential density, and physical height. f is the Coriolis frequency, g gravity, θ_0 a reference potential temperature or density, and N is the buoyancy, or Brunt-Väisälä, frequency which is defined from the background time and horizontally independent stratification $\langle\theta\rangle$ by

$$N^2 = \frac{g}{\theta_0}\frac{d\langle\theta\rangle}{dz}. \tag{7}$$

The vertical dependence of Eqs. (2)–(6) can be separated from the horizontal dependence by assuming

$$\psi, \chi, \phi \propto F(z), \quad \theta \propto \frac{dF}{dz}, \quad w \propto \frac{dF/dz}{N^2}. \tag{8}$$

The vertical structure function F satisfies the equation

$$\frac{d}{dz}\left(\frac{dF/dz}{N^2}\right) + \frac{F}{\lambda^2} = 0, \tag{9}$$

where λ is the separation constant, which has the dimension of velocity. The simplest vertical boundary conditions would be

$$\frac{dF}{dz} = 0 \quad \text{on} \quad z = z_s \text{ and } z_a, \tag{10}$$

corresponding to zero vertical velocity at the rigid, flat upper and lower boundaries. If $N^2 > 0$ everywhere, the vertical structure functions form a complete, orthogonal basis set, and the set of eigenvalues $\{\lambda_n\}$ is discrete with λ_n decreasing monotonically as n increases.

The hydrostatic, continuity and heat equations (4)–(6) can be combined into the single equation,

$$\phi_t + \lambda_n{}^2\nabla^2\chi = 0, \tag{11}$$

which, along with the vorticity and divergence equations (2) and (3), describe the linear waves of the BE. For the gBE model the governing equations are (2), (11) and

$$\textit{Divergence} \qquad \nabla\cdot(f\nabla\psi) + J(f, \chi) = \nabla^2\phi, \tag{12}$$

see Gent and McWilliams (1983a). We also restrict our analysis to an equatorial β-plane, and thus set

$$f = \beta y. \tag{13}$$

We follow Moore and Philander (1977) and non-dimensionalize for each vertical mode by assuming the following scales:

$$\left.\begin{aligned} x, y &\sim (\lambda_n/\beta)^{1/2}, \quad \psi, \chi \sim (\lambda_n{}^3/\beta)^{1/2} \\ t &\sim (\lambda_n\beta)^{-1/2}, \quad \phi \sim \lambda_n{}^2 \end{aligned}\right\}. \tag{14}$$

This is equivalent to setting Lamb's parameter equal to unity in the Laplace Tidal equations.[3] We assume wavelike solutions, with all variables

$$\propto \exp[i(kx - \omega t)], \quad c = \omega/k. \tag{15}$$

The equations assume their most convenient form when stated in terms of the variables v and Φ where

$$v = \psi_x + \chi_y, \quad \Phi = -\phi_t. \tag{16}$$

The linearized BE can then be shown to take the following form:

$$v_{yy} - (k^2 + 1/c)v = \Phi_y + y\Phi/c, \tag{17}$$

$$BE \quad cv_y + yv = \Phi_{yy} + (c - k^2 - y^2)\Phi + ck^2\chi, \tag{18}$$

$$\chi_{yy} - k^2\chi = \Phi. \tag{19}$$

[3] A direct comparison between our results and Moura's (1976) results can be made by the correspondences $\phi \equiv \Phi$, $\omega \equiv \epsilon^{1/4}\lambda$, $k \equiv \epsilon^{-1/4}s$, and $y \equiv \eta = \epsilon^{1/4}$ sin(latitude).

The linearized gBE equations are (17), (19) and

$$gBE \qquad cv_y + yv = \Phi_{yy} + (c - k^2 - y^2)\Phi. \qquad (20)$$

We have shown in Gent and McWilliams (1983a) that there are several choices of boundary conditions for balanced models in a bounded domain. In Appendix A of that paper we listed two choices for the BE, which, when linearized on an equatorial β-plane, are

$$BE\text{: Choice 1} \qquad \psi_x = \chi_y = 0, \quad \phi_y = y\psi_y, \quad \text{on} \quad y = \pm L, \qquad (21)$$

$$BE\text{: Choice 2} \qquad \psi_x + \chi_y = 0, \quad \phi_x = \psi_{yt}, \quad \phi_y = y\psi_y, \quad \text{on} \quad y = \pm L. \qquad (22)$$

In terms of v, Φ, and χ, these boundary conditions become

BE: Choice 1

$$\left.\begin{aligned} v = 0, \quad \chi_y = 0, \\ \Phi_y = cy[v_y - k^2\chi - \Phi] \end{aligned}\right\}, \quad \text{on} \quad y = \pm L, \qquad (23)$$

BE: Choice 2

$$\left.\begin{aligned} v = 0, \quad \Phi_y = -y\Phi/c, \\ v_y = \Phi(1 - c^{-2}) + k^2\chi \end{aligned}\right\}, \quad \text{on} \quad y = \pm L. \qquad (24)$$

For the gBE model there are again two choices. They are (21) and (22), except that

$$gBE \qquad \phi_y = y(\psi_y - \chi_x), \quad \text{on} \quad y = \pm L, \qquad (25)$$

replaces the final condition in each. In terms of v, Φ, and χ the boundary conditions become

$$gBE\text{: Choice 1} \qquad v = 0, \quad \Phi_y = cy(v_y - \Phi), \quad \chi_y = 0, \quad \text{on} \quad y = \pm L, \qquad (26)$$

gBE: Choice 2

$$\left.\begin{aligned} v = 0, \quad \Phi_y = cy(v_y - \Phi) \\ ck^2\chi = \Phi_y/y + \Phi/c \end{aligned}\right\}, \quad \text{on} \quad y = \pm L. \qquad (27)$$

For the gBE, Eq. (20) and the first two boundary conditions in (26) and (27) do not involve χ. Thus, when $k \neq 0$, the χ problem is purely diagnostic because the homogeneous solution of (19) can be used to satisfy either of the χ boundary conditions in (26) or (27). (The $k = 0$ problem is a subtle exception; see Appendix A.) Therefore, the gBE eigenvalue problem is only a function of the two variables v and Φ and is independent of the choice of boundary conditions. In contrast, the BE problem does involve χ and is influenced by the choice of boundary conditions (23) or (24). On the infinite equatorial β plane, the boundary conditions imposed are

$$BE, gBE \qquad v, \Phi \to 0, \quad \text{as} \quad |y| \to \infty. \qquad (28)$$

b. Methods

As for the PE, the equatorial waves of the BE and gBE split into symmetric modes with Φ and χ symmetric and v antisymmetric in y, and antisymmetric modes which have the opposite symmetries in y. For each mode this implies the appropriate symmetry conditions at the equator $y = 0$. On a finite β-plane, the eigenvalues, for a given value of k^2, were determined by a "shooting" method which yields a nonlinear system of equations whose zeros were found by the secant method. This system involves two equations for the gBE and three for the BE. The method involves integration of ordinary differential equations which was done by a 5th–6th order Runge–Kutta technique. The calculated eigenvalues are accurate to at least three significant figures.

For the results on the infinite equatorial β-plane we expand the variables in the complete, orthonormal basis set of Hermite functions such that

$$\left.\begin{aligned} v = \sum_{m=0}^{M} v_m G_m, \quad \Phi = \sum_{m=0}^{M} \Phi_m G_m \\ \chi = \sum_{m=0}^{M} \chi_m G_m \end{aligned}\right\}. \qquad (29)$$

The Hermite functions G_m are defined by

$$G_m = \frac{H_m e^{-y^2/2}}{(2^m m! \pi^{1/2})^{1/2}}, \qquad (30)$$

where H_m is the Hermite polynomial of degree m. This reduces the differential equations to algebraic equations, which can be combined into the following recursion relations for the v_m's:

$$BE \qquad v_{m-4}C_{m-4} + v_{m-2}C_{m-2} + v_m C_m + v_{m+2}C_{m+2} + v_{m+4}C_{m+4} = 0, \qquad (31)$$

$$gBE \qquad v_{m-2}C^1_{m-2} + v_m C^1_m + v_{m+2}C^1_{m+2} = 0. \qquad (32)$$

The C and C^1 represent coefficients in the recursion relations; they and the diagnostic relations for Φ_m are given in Appendix B. The technique used to calculate the eigenvalues was a form of shooting: for example, for the first Rossby wave k^2 was chosen, v_1 was set to an arbitrary normalization value, and values for v_3 and c were guessed. The BE recursion relation (31) for $m \geq 1$ was then used to evaluate all the other coefficients to v_M, and higher coefficients were set to zero. The two residuals, found by evaluating the lhs of (31) when $m = M - 2$ and M are zero for an eigensolution, and their values were used to adjust the guesses for v_3 and c until an eigensolution was obtained by iteration. The gBE solutions were easier to obtain because Eq. (32) only involves three v coefficients so that only the eigenvalue c had to be guessed in the shooting technique iteration. This technique relies on a finite sum to M in Eq. (29), but in all cases

we checked our results by finding that they were insensitive to the truncation level. The convergence rate of solutions of the form (29) is moderate when k^2 is O(1), but becomes very slow as k^2 gets small. In fact, the number of terms in the series (29) needed for reasonable accuracy becomes extremely large as $k^2 \to 0$. Thus any finite M calculation is not valid for small enough k^2, and in the following sections we only plot the infinite domain dispersion curves down to the value of k^2 valid for calculations with the highest value of M attempted, which is 640 or 641. Thus, this solution technique is unable to address the precise form of the infinite domain dispersion curves as $k^2 \to 0$. Satisfying the boundary conditions (28) requires that

$$v_m, \Phi_m = O(m^{-1/4}) \quad \text{as} \quad m \to \infty, \tag{33}$$

because a constant has an asymptotic series proportional to $m^{-1/4}$ as $m \to \infty$.

3. Analytic results

a. General

In this section we present some analytic results for the equatorial waves of the BE and gBE on an infinite and finite equatorial β-plane. The section follows fairly closely the analytic work of Moura (1976) for the Laplace tidal equations on a sphere. We assume that

$$(\psi, \chi, \phi) = \mathrm{Re}(P, iQ, R) \exp[i(kx - \omega t)]. \tag{34}$$

Multiplying (i) the vorticity equation (2) by the complex conjugate of P, P^*, (ii) the divergence equation (12) with α multiplying the Jacobian term by $-iQ^*$, and (iii) the non-dimensional form of Eq. (11) by $-R^*$, adding and integrating, we obtain

$$\begin{aligned}\omega \int_{-L}^{L} \{|P_y|^2 + |R|^2 + k^2|P|^2\} dy \\ = k \int_{-L}^{L} \{\alpha|Q|^2 - |P|^2\} dy \\ + [\omega P_y P^* + y(P_y Q^* - Q_y P^*) \\ + Q_y R^* - R_y Q^*]_{y=-L}^{y=L},\end{aligned} \tag{35}$$

where $\alpha = 0$ for the BE and $\alpha = 1$ for the gBE. For the BE on an infinite β-plane, or with Choice 1 boundary conditions (21) on a finite β-plane, the boundary terms in (35) are zero. Using the convention that ω is always positive, Eq. (35) then shows that there are no eastward traveling waves with k positive. For the BE with Choice 2 boundary conditions (22), the rhs of (35) reduces to

$$2k\{L|P|^2(L) - (PR^* + P^*R)(L) - \int_0^L |P|^2 dy\}. \tag{36}$$

Thus, eastward traveling waves cannot be ruled out *a priori*, but in extensive numerical searches we have not found any (see Section 5). Thus the BE have no eastward traveling waves, and in particular no equivalent of the Kelvin wave. For the gBE, however, $\alpha = 1$ in (35) and eastward traveling waves are possible. On an infinite β-plane the boundary terms in (35) are again zero so that these waves must have strong divergence in the sense that

$$\int_{-\infty}^{\infty} \{|Q|^2 - |P|^2\} dy > 0. \tag{37}$$

b. The long-wave limit

We now examine the equations in the limit of very long and slow waves: set ω and $k = 0$ such that c is finite.[4] In this limit v, Φ, and χ are all O(1), and both the gBE and BE on an infinite β-plane possess the solutions

$$v = G_m(y),$$

$$\Phi = \frac{-1}{2\sqrt{2}} [(m+1)^{-1/2} G_{m+1} + m^{-1/2} G_{m-1}],$$

$$c = -(2m+1)^{-1}; \quad \text{Rossby waves,} \tag{38}$$

$$\Phi = G_0(y), \quad v \equiv 0, \quad c = 1; \quad \text{Kelvin wave.} \tag{39}$$

These are identical to the Rossby and Kelvin wave solutions of the PE.

In the last subsection it was shown that the BE in an infinite domain do not possess a Kelvin wave when ω and k are non-zero so that the long wave limit is singular in this particular case. This type of singularity we call non-existence for $k \neq 0$, and it is listed in Table 1, which gives the various types of singularity near $k = 0$ for all waves. Numerical computation also suggests that all the above waves are singular in this limit for the gBE in an infinite domain. This type of singularity we call infinite slope in Table 1 because plots of c against k^2 have infinite slope at $k^2 = 0$. Since

$$\frac{dc}{dk^2} = \frac{\left(\frac{d\omega}{dk} - c\right)}{2k^2}, \tag{40}$$

it implies that these long waves are dispersive because their group and phase velocities are unequal. The antisymmetric Rossby waves of the BE in an infinite domain also have infinite slope in this limit, but the symmetric Rossby waves have another type of singularity which we call discontinuous c in Table 1. This means that the c against k^2 curve has a finite gradient as $k^2 \to 0$, but the limiting value of c is not

[4] The long and short wave limits, $k \to 0$ and ∞, are the same as letting the Lamb parameter $\epsilon \to \infty$ and 0 in Moura's (1976) work.

the $k^2 = 0$ value. The numerical evidence for these long-wave limit singularities, and the behavior in a finite domain are documented in Sections 5 and 6, and the limit is discussed in detail in Appendix A.

c. Short Rossby waves

The next limit we consider is the short, westward traveling Rossby waves with $-k \to \infty$ and $\omega \to 0$. A solution of both gBE and BE on an infinite β-plane is

$$\left.\begin{aligned} v &= G_m(y) + O(k^{-2}) \\ \Phi &= -yv/k^2 + O(k^{-4}) \\ \chi &= yv/k^4 + O(k^{-6}) \\ c^{-1} &= -(k^2 + 2m + 1) + O(k^{-2}) \end{aligned}\right\} . \quad (41)$$

This is the same as the PE limit, so that, to this order of accuracy, the BE and gBE short Rossby waves are those of the PE. Moura (1976) also shows this behavior for the short Rossby waves of the Laplace tidal equations. The limit is confirmed by the numerical results on the infinite equatorial β-plane.

d. gBE spurious waves

The final limit we consider is short, eastward traveling waves in the gBE with k and $\omega \to \infty$. Then a solution of (17), (19), and (20) in an infinite domain is

$$\left.\begin{aligned} \Phi &= G_m(y/2^{1/4}) + O(k^{-2}) \\ v &= -\Phi_y/k^2 + O(k^{-4}) \\ \chi &= -\Phi/k^2 + O(k^{-4}) \\ c &= k^2 + \sqrt{2}(2m + 1) + O(k^{-2}) \end{aligned}\right\} . \quad (42)$$

This is the infinite equatorial β-plane equivalent of Moura's result (7.5) on the sphere, where again $c \approx k^2$ to leading order in k. These are spurious, very high frequency waves that have no counterpart in the BE or PE. This limit (42) in the gBE is confirmed by numerical calculations (see Section 6). These spurious waves are not like PE gravity waves because they are highly dispersive since their group velocity is three times the phase velocity as $k \to \infty$. They are also almost purely divergent with $\psi \approx \chi k^{-3}$, and thus satisfy the inequality (37).

4. The primitive equation dispersion relation

The PE dispersion relation is

$$\omega^2 - \frac{k}{\omega} - k^2 = 2\mu_m + 1, \quad (43)$$

where μ_m equals m in an infinite basin and is very close to m in a wide, but finite basin. Cane and Sarachik (1979) show that the difference between μ_m and m is of order $(2^{1/2}L)^{2m+1}e^{-L^2}$ for mode m, or $O(10^{-8})$ for the first Rossby wave when $L = 5$. Thus, the Rossby and gravity wave dispersion curves are essentially identical, and the Kelvin wave curve is identical for $L = 5$ and for an infinite domain. These curves are labeled R, G and K, respectively, in Fig. 1, which is the dispersion diagram for $L = 5$. In an infinite domain the mixed Rossby–gravity wave is described by

$$v = G_0(y), \quad \Phi = -\omega^2 G_1 2^{-1/2}, \quad k = \omega - \frac{1}{\omega} . \quad (44)$$

However, in a finite domain this wave splits into separate high and low frequency components which are both labeled MRG in Fig. 1. The high and low frequency dispersion curves are asymptotic to ω, $-k \to \infty$, and to ω, $-k \to 0$, respectively, such that $c \to -1$. Both components of the mixed Rossby–gravity wave are antisymmetric and are separated by the dispersion curve of the symmetric anti-Kelvin wave. It has

$$\Phi = \exp\left(\frac{y^2}{2}\right), \quad v \equiv 0, \quad c = -1, \quad (45)$$

but is not shown in Fig. 1 because it would be confusing in the diagram since it lies so close to the mixed Rossby–gravity components when $L = 5$. The anti-Kelvin wave can be interpreted as a coastal Kelvin wave near the boundaries $y = \pm L$. In subsequent figures, some PE curves are reproduced for comparison; they are always the dotted curves.

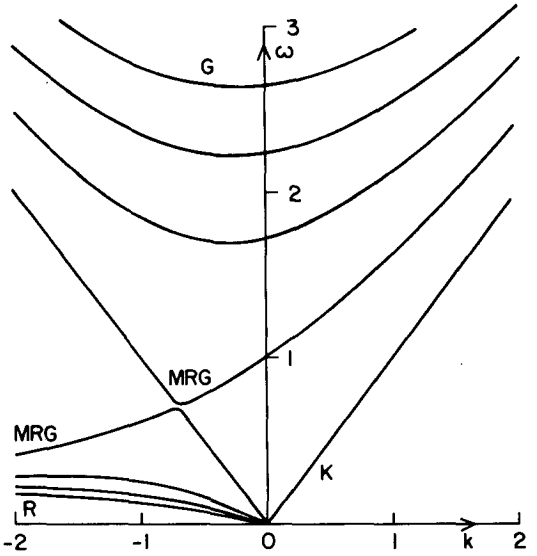

FIG. 1. The dispersion diagram of primitive equation equatorial waves in a bounded domain with $L = 5$. G, R, K, and MRG are the gravity, Rossby, Kelvin (symmetric) and the high and low frequency components of the mixed Rossby–gravity wave (antisymmetric). The anti-Kelvin wave (symmetric), with $\omega = -k$, is not shown because it is so close to the MRG curves. PE curves are reproduced as dotted lines in all the following figures.

5. The balance equations—numerical results

a. Finite domain

The first case we examine is the BE in a finite domain with Choice 1 boundary conditions. In this situation there are no eastward traveling waves (see Section 3). Figure 2 shows the BE version of the westward traveling first three Rossby waves and mixed Rossby–gravity wave when $L = 5$. Comparison with Fig. 1 shows that this mixed Rossby–gravity wave is probably best thought of as the equivalent of the low frequency part of the PE mixed Rossby–gravity wave. The reason is that it approaches the origin such that $c \to -1$ as $\omega, -k \to 0$, and the eigenfunctions are similar in this limit. There is no equivalent of the PE high frequency component of the mixed Rossby–gravity and anti-Kelvin waves. This is not surprising because it is shown in Appendix A of Gent and McWilliams (1983a) that Choice 1 boundary conditions for the BE excise boundary-trapped waves. Thus, in the long-wave limit, there is no equivalent of the PE mixed Rossby–gravity wave with eastward group velocity. This remains true for larger values of L when the mixed Rossby–gravity curve follows the PE infinite domain curve closer to the ω axis, but still has a maximum in ω and approaches the origin with $c \to -1$.

The BE dispersion diagram with Choice 2 boundary conditions for $L = 5$ is shown in Fig. 3. The low frequency component of the mixed Rossby–gravity wave is very close to the PE curve. The high frequency mixed Rossby–gravity curve lies above the PE curve for relatively small ω, but then drops into the origin at a very steep angle, with the value of c depending upon L. For larger values of L the local maximum in this curve occurs at a higher value of ω and closer

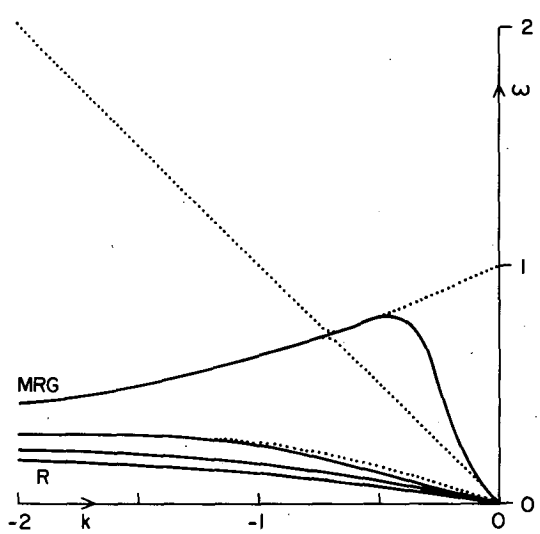

FIG. 2. The dispersion diagram of the BE with Choice 1 boundary conditions and $L = 5$.

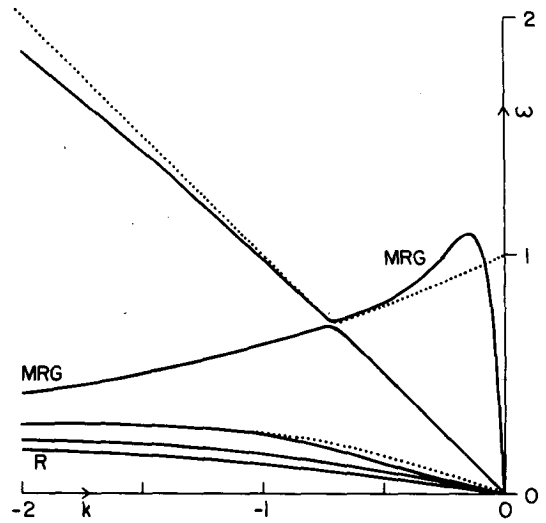

FIG. 3. As in Fig. 2 but with Choice 2 boundary conditions and $L = 5$. The anti-Kelvin wave (symmetric) is not shown because it is so close to the two components of the MRG wave (antisymmetric).

to the ω axis, but it still eventually goes to the origin with increasing values of $-c$. Thus, the group velocity of this wave is again westward in the long-wave limit, but, for a given value of L, it is westward over a much smaller interval of k than for Choice 1 boundary conditions. When $L = 5$ the intervals are approximately $-0.14 < k < 0$ for Choice 2 and $-0.45 < k < 0$ for Choice 1 boundary conditions. Choice 2 boundary conditions for the BE retain boundary-trapped waves (Gent and McWilliams 1983a, Appendix A), and the BE do have an anti-Kelvin wave in this case. This symmetric wave is not shown in Fig. 3, but it separates the two components of the antisymmetric mixed Rossby–gravity wave. It and the low frequency component both approach the origin with $c \to -1$ irrespective of the value of L, but its $\omega, -k \to \infty$ asymptote, which is the same as that of the high frequency component, depends somewhat upon L.

With both sets of boundary conditions an infinite set of Rossby waves occurs in the BE in a finite domain. The first three Rossby waves for the two choices and $L = 5$ are plotted on Figs. 2 and 3. The dispersion curves and those of the PE are very close when $-k$ is large and gradually separate as $-k$ gets smaller. The first Rossby wave is the only one which, on plots with the scale of Figs. 2 and 3, is distinguishable from the PE curve. Differences between the curves are accentuated on a plot of c against k^2 for small values of k^2, which is shown in Fig. 4 for the first Rossby mode. All calculations in finite domains are accurate to $k^2 = 10^{-4}$. This shows that the dispersion curves for the two choices of boundary conditions are close as $k^2 \to 0$, and both diverge considerably from the PE curve. For both sets of boundary conditions the long-

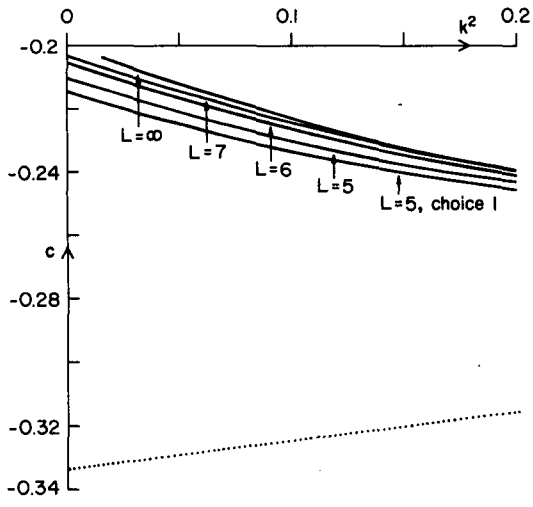

FIG. 4. A plot of c against k^2 for the first Rossby wave of the BE. The curves are for $L = 5$ with both choices of boundary conditions, for $L = 6$ and 7 with choice 2 boundary conditions, and for $L = \infty$.

wave limit has a discontinuity in c because the limiting value of c is not equal to the $k^2 = 0$ value given in Eq. (38). The limiting value of c depends upon L, as can be seen from the Choice 2 boundary condition curves for $L = 6$ and 7 which are also plotted in Fig. 4. As L increases for both sets of boundary conditions the limiting value of c tends towards the $k^2 = 0$ value for the next gravest BE antisymmetric mode, in this case the second Rossby wave with c very close to -0.2 at $k^2 = 0$. This is true for all other symmetric Rossby modes which also have a discontinuous c singularity in the long-wave limit as $\omega, -k \to 0$ (see Table 1). However, the antisymmetric modes are regular in this limit, with the value of c as $k^2 \to 0$ tending toward the $k^2 = 0$ value. This can be seen in Fig. 5 which is a plot of c against k^2 for the second Rossby wave dispersion curves for both choices of boundary conditions when $L = 5$ and for Choice 2 boundary conditions when $L = 6$ and 7. Unlike the mixed Rossby–gravity wave, the group velocity properties of the BE Rossby waves are very similar to those of the PE.

b. *Infinite domain*

We now consider the BE on an infinite equatorial β-plane. There are no eastward traveling waves, and the westward traveling ones are shown in Fig. 6. It shows the mixed Rossby–gravity wave and the first three Rossby waves. For large negative k the dispersion curves are very close to the infinite basin PE curves. As $-k$ reduces, noticeable differences first occur in the first Rossby wave and then in the mixed–Rossby gravity wave, whereas on the scale of Fig. 6, the higher Rossby waves do not show any differences. We have terminated the mixed Rossby–gravity curve at $k \approx -0.14$ because this is the smallest value of $-k$ where our calculations are accurate. As described in Section 3, the series in Eq. (29) are very slowly convergent as $k^2 \to 0$, and we only plot results where they are valid for the highest values of M used. It appears from our computations with increasing values of M that the BE curve continues towards the ω axis slightly above the PE curve with ω remaining finite as k^2 becomes small.

The Rossby wave curves in Fig. 6 are only valid to $k \approx -0.12$, as is demonstrated in Fig. 7 which is a plot of c against k^2 for the first Rossby wave with

TABLE 1. Singularity types near $k = 0$.

	Finite domain			Infinite domain	
Wave	BE Choice 1 boundary conditions	BE Choice 2 boundary conditions	gBE	BE	gBE
Kelvin	Does not exist for $k \neq 0$	Does not exist for $k \neq 0$	Discontinuous c	Does not exist for $k \neq 0$	Infinite** slope
Anti-Kelvin	Does not exist for $k \neq 0$	Regular	Discontinuous c	—*	—*
High-frequency mixed Rossby–gravity	Does not exist for all k	Does not exist for $k = 0$	Infinite c	Does not exist for $k = 0$	Infinite c
Low-frequency mixed Rossby–gravity	Regular	Regular	Regular	—*	—*
Symmetric Rossby	Discontinuous c	Discontinuous c	Discontinuous c	Discontinuous c	Infinite** slope
Antisymmetric Rossby	Regular	Regular	Regular	Infinite slope**	Infinite** slope

* — Means there is no such wave in BE, gBE and PE.
** Infinite slope means $|dc/dk^2| \to \infty$ as $k^2 \to 0$.

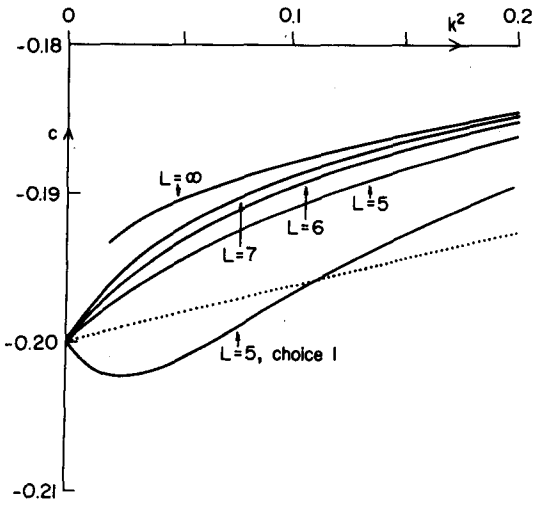

FIG. 5. As in Fig. 4 but for the second Rossby wave of the BE. The curves are for $L = 5$ with both choices of boundary conditions, for $L = 6$ and 7 with choice 2 boundary conditions, and for $L = \infty$.

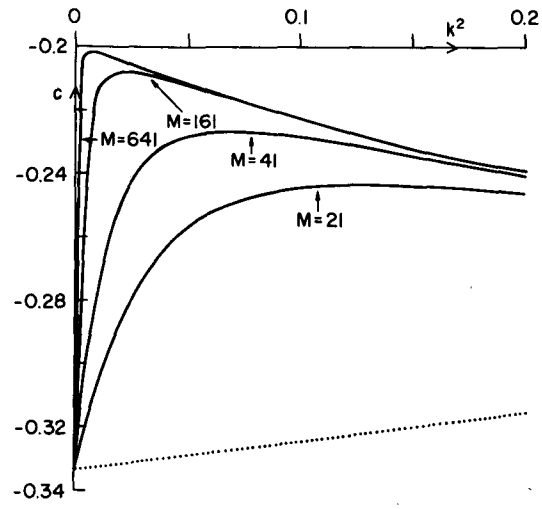

FIG. 7. As in Fig. 4 but for the first Rossby wave of the BE in an infinite domain for various truncations in Eq. (29). The curves are for $M = 21$, 41, 161, and 641.

various values of M. As $k^2 \to 0$ each individual curve tends to the $k^2 = 0$ limit of $c = -\frac{1}{3}$, but the infinite domain curve appears to have c tending to -0.2 as $k^2 \to 0$. This interpretation is consistent with the curves for a finite domain as L increases. This can be seen from Fig. 4 where the infinite domain $M = 641$ curve is reproduced down to the smallest value of k^2 where it is valid. Thus the symmetric Rossby waves have a discontinuity in c because the limiting value of c is not the $k^2 = 0$ value but rather the $k^2 = 0$ value of the next gravest antisymmetric Rossby wave. However, they are nondispersive in the long-wave limit because the gradient of c against k^2 is finite.

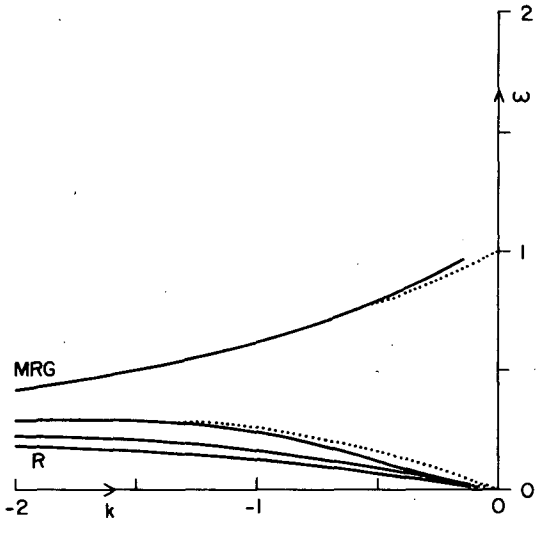

FIG. 6. As in Fig. 2 but in an infinite domain.

The antisymmetric Rossby waves behave differently in the long-wave limit. Figure 5 shows c versus k^2 for increasing values of L and the infinite domain curve for k^2 down to ≈ 0.017. The consistent interpretation is that, in an infinite domain, the limiting value of c is -0.2 but that it is approached with infinite positive gradient as $k^2 \to 0$. We have called this type of singularity infinite slope in Table 1. This applies to all antisymmetric Rossby waves and by Eq. (40) implies they are dispersive in the long wave limit. Thus, compared to the PE, all BE Rossby waves on an infinite β-plane are singular in the long-wave limit. A more detailed analysis of the different types of singularities is in Appendix A.

We can compare these infinite basin results to Moura's (1976) results for the BE over a spherical domain. We agree with Moura in that there are only westward traveling waves, that in the short-wave limit the BE results are very close to those of the PE, that in the long-wave limit the mixed Rossby–gravity wave frequency is slightly larger than the PE value, and that, in this limit, the Rossby waves group in pairs tending to the $k^2 = 0$ limit of the antisymmetric wave (see Moura's Fig. 9). However, Moura varied the wavenumber by less than an order of magnitude and did not address the singularities in the long-wave limit.

6. The global balance equations—numerical results

a. Finite domain

We first examine the gBE in a finite domain. The results for $k \neq 0$ are the same for both sets of boundary conditions because the χ problem is purely diagnostic. Both sets of boundary conditions allow boundary

trapped waves, so we expect the mixed Rossby–gravity wave to split into two, and the anti–Kelvin wave to be present. This is indeed the case and the two Rossby–gravity components are shown in Fig. 8, which is the gBE dispersion diagram when $L = 5$. The low frequency component is very close to the PE curve and is regular at the origin. The high frequency component of the mixed Rossby–gravity wave has yet another type of singularity in the long-wave limit. In Table 1 it is called infinite c because the curve has $\omega \to \infty$ as $-k \to 0$. This is different from the BE where it goes into the origin as $-k \to 0$. Thus, in the long-wave limit the gBE frequency is much larger than that of the PE, but the gBE do preserve the fact that the group velocity is eastward in this limit, in contrast to the BE. Comparing Figs. 2, 3 and 8 there is an intermediate range, $-1 < k < -0.5$, or to smaller $-k$ with Choice 2 boundary conditions, where the BE mixed Rossby–gravity curve is closer to the PE one than that of the gBE. The symmetric anti-Kelvin wave is not shown in Fig. 8, but again it separates the two components of the antisymmetric mixed Rossby–gravity wave. Unlike the BE, the anti–Kelvin wave has a discontinuous c singularity near the origin with $c \to -1.05$ as $\omega, -k \to 0$. It diverges further from the PE curve as $-k$ increases, and its asymptote, as ω, $-k \to \infty$ which is the same as that of the high frequency component, depends upon the value of L.

Like the BE, the gBE have an infinite set of Rossby waves, the first of which is shown in Fig. 8. Comparison with Figs. 2 and 3 shows that this wave in the gBE is a much better approximation to the PE wave than its BE counterpart. Like the BE, however, all symmetric Rossby waves have a discontinuous c singularity in the long-wave limit as $-k \to 0$. This can be seen for the first Rossby wave in Fig. 9, which is a plot of c against k^2 for small k^2 and $L = 5$, 6, and 7. The three limiting values of c as $k^2 \to 0$ are not the expected $k^2 = 0$ gBE and PE value of $-\frac{1}{3}$. The value of c at $k^2 = 0.2$ is almost independent of L, but the limiting value as $k^2 \to 0$ is dependent upon L. However, it tends towards the $k^2 = 0$ value of $-\frac{1}{3}$ as L increases. These values of c for small k^2 for the gBE are much closer to the PE values than their BE counterparts, so that on the scale of Fig. 8 the gBE curve is indistinguishable from the PE curve. The antisymmetric Rossby waves are again regular in the long-wave limit, and this difference between symmetric and antisymmetric modes is analyzed in more detail in Appendix A.

Fig. 8 also shows that the gBE have a Kelvin wave which for small values of ω and k is close to its PE counterpart. It also has a discontinuous c singularity in the long-wave limit, and its behavior is like that of the symmetric Rossby waves. This can be seen from Fig. 10, which is a plot of c against k^2 for $L = 5$, 5.5 and 6. Again the limiting value of c as $k^2 \to 0$ depends upon L, and it tends towards the $k^2 = 0$ gBE and PE value of 1 as L increases. Thus the gBE have an eastward traveling symmetric mode, and its group velocity is everywhere eastward. The dispersion curve diverges quickly from the PE curve, and the frequency becomes much larger than that of PE gravity waves as k increases. Finally, Fig. 8 shows the first of an infinite set of spurious, very-high frequency eastward traveling waves. Its minimum frequency value is greater than five, and it is asymptotic to $\omega \to \infty$ as $k \to 0$ and to near the Kelvin mode as $k \to \infty$. The exact position and minimum value of this mode are quite dependent upon the value of L. These spurious waves are not like the PE gravity

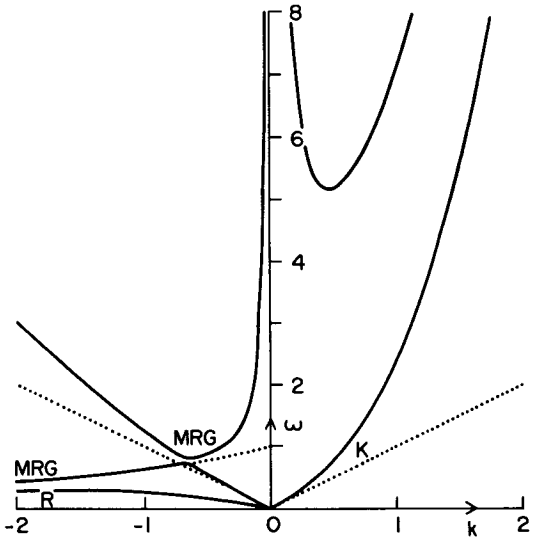

FIG. 8. The dispersion diagram of the gBE for both choices of boundary conditions and $L = 5$. The anti–Kelvin wave (symmetric) is not shown because it is so close to the two components of the MRG wave (antisymmetric).

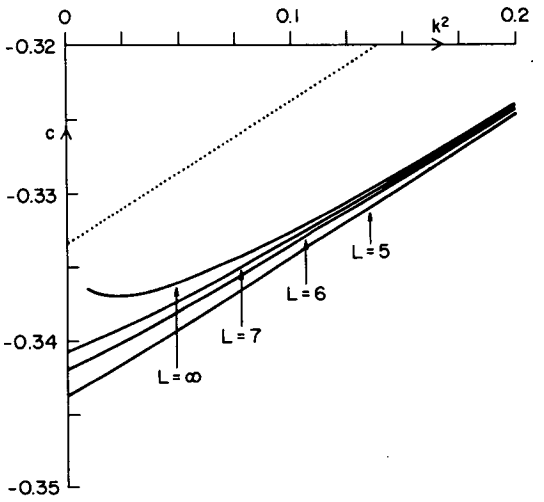

FIG. 9. As in Fig. 4 but for the first Rossby wave of the gBE. The curves are for $L = 5$, 6, 7, and ∞.

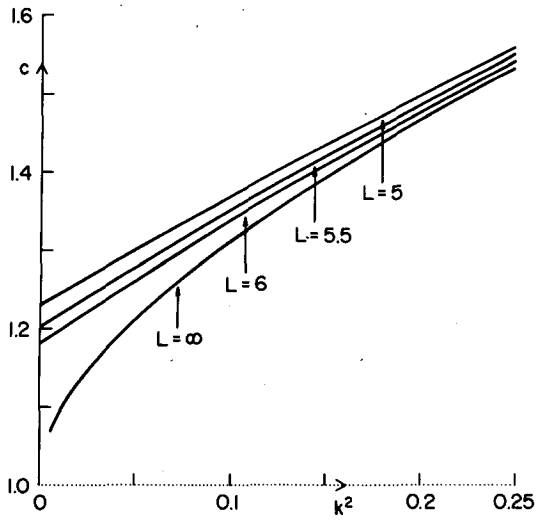

FIG. 10. As in Fig. 4 but for the Kelvin wave of the gBE. The curves are for L = 5, 5.5, 6 and ∞.

waves and are discussed more fully in the infinite domain case below.

b. *Infinite domain*

The gBE dispersion diagram on an infinite equatorial β-plane in the range $0 < \omega < 3$ is shown in Fig. 11. The mixed Rossby–gravity wave does not split into two, and there is no anti-Kelvin wave. As in Fig. 6 for the BE, the mixed Rossby–gravity curve is only continued as far as it is valid, which is $k \approx -0.07$. It is clear, however, that it has an infinite c singularity in the long-wave limit with $\omega \to \infty$ as $-k \to 0$. This is in contrast to its BE counterpart where ω remains finite. As in a finite basin, there is a distinct range of small $-k$ where the BE curve is a better approximation to the PE mixed Rossby–gravity curve than the gBE curve. The first three of the infinite set of Rossby waves are shown in Fig. 11, and they are very close to the PE curves. They are valid down to $k \approx -0.1$ as can be seen from Fig. 9, which shows the first Rossby wave on a plot of c against k^2. Each curve for a finite M truncation tends to the limit of $-\frac{1}{3}$ as $k^2 \to 0$ with increasing negative gradient as M increases. An interpretation, consistent with the above and the curves for increasing values of L in Fig. 9, is that the infinite domain curve has an infinite slope singularity. This means that it $\to -\frac{1}{3}$ as $k^2 \to 0$ but with infinite negative gradient. The other gBE symmetric Rossby waves behave similarly, in contrast to those of the BE, see Table 1 and Fig. 4. However, the gBE antisymmetric Rossby waves behave like their BE counterparts in Fig. 5. The long-wave limit is regular for all finite values of L, but the infinite domain curve has an infinite slope singularity. These infinite gradients imply that all the infinite domain gBE Rossby waves are dispersive in the long-wave limit (see Eq. 40).

The gBE Kelvin wave also has an infinite slope singularity in the long-wave limit. This can be seen in Fig. 10 which is a plot of c against k^2 for increasing values of L and for an infinite domain. The last curve appears to be tending to unity with infinite gradient. The Kelvin wave quickly diverges from its PE counterpart with $c = 1$ as k increases, and the positive k dispersion diagram with ω to 25 is shown in Fig. 12. It also shows the first three members of the infinite set of spurious waves. Again as $k \to 0$, the plots are only continued as far as they are valid, but all these

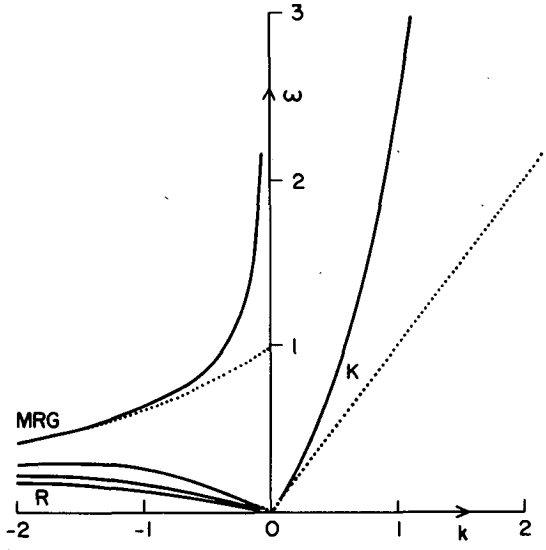

FIG. 11. As in Fig. 8 but in an infinite domain for small frequencies.

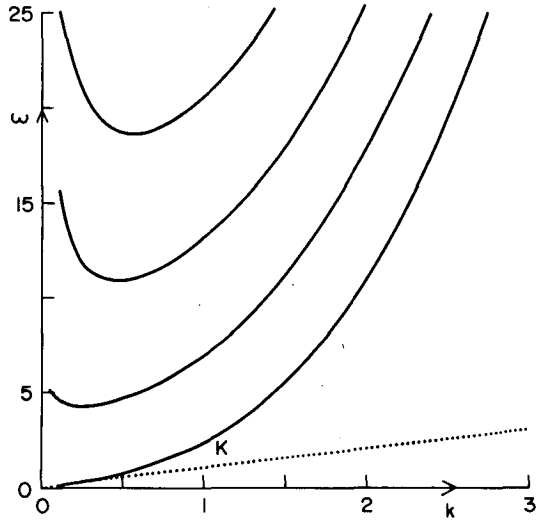

FIG. 12. As in Fig. 11 but for positive wavenumbers and large frequencies.

waves have $\omega \to \infty$ as $k \to 0$. We have been unable to find analytic, asymptotic expressions for these waves in this limit. For the first of these spurious modes the value and position of the minimum is finitely different from the $L = 5$ value shown in Fig. 8. As $\omega, k \to \infty$, the Kelvin wave and the spurious waves are described by the asymptotic expressions in Eq. (42) with $m = 0, 1, 2, \ldots$.

We can again compare these results with those of Moura (1976). We agree with his conclusions in the long-wave limit: that the mixed Rossby–gravity frequency is greater than the primitive equation frequency and that the gBE Rossby wave c values tend towards the PE values (see his Fig. 26). Thus the gBE Rossby waves are better approximations to those of the PE than are the BE waves. Moura also showed that the Kelvin and spurious wave frequencies increase rapidly as k increases (see his Fig. 25), and identified the $c \approx k^2$ limit as $k \to \infty$ [his Eq. (7.5)]. Again he did not address the long-wave limit singularities.

7. Conclusion

The BE have no eastward traveling waves on the equatorial β-plane. The only high frequency waves are the anti-Kelvin wave and the high frequency component of the mixed Rossby–gravity wave with Choice 2 boundary conditions in a finite domain. The major error of the BE dispersion diagram relative to the low frequency PE is that there are no long waves with eastward group velocity. This would be a severe handicap in trying to model the large-scale, slow equatorial response to transient forcing, for example. The BE have an infinite set of Rossby waves, but their behavior, especially the first wave, is somewhat different in the long-wave limit than in the PE.

In contrast to the BE, the gBE have both symmetric and antisymmetric waves with eastward group velocity in the long-wave limit. This would be a definite advantage in simulating the transient equatorial response to wind forcing when these waves are important. The gBE also have somewhat better long Rossby waves than the BE, so that the very long wave response will be more accurate. There is an intermediate range of wavenumber, however, where the BE mixed Rossby–gravity wave is a better approximation than its gBE counterpart. The major disadvantage of the gBE is that they have not eliminated all high frequency modes, and that they have the Kelvin, high frequency component of the mixed Rossby–gravity and spurious modes with much higher frequencies than the gravest PE gravity waves. In a numerical model with an explicit time-stepping algorithm, this would entail taking much smaller time steps for the gBE than for the PE. However, an implicit time stepping scheme can probably be found that eliminates these very high frequency waves and allows longer time steps, as has been done for the PE (see e.g., Simmons *et al.*, 1978).

Our conclusion is that balanced models, especially the gBE, have useful solutions in domains which span the equator. We have shown that their equatorial waves are not quite those of the PE in the long-wave limit, but this is outweighed by other attributes of balanced models. These include their retention of some nonlinear terms, which would give a more realistic equatorial undercurrent than a linear PE model for example, and their regimes of validity at midlatitudes. However, if the sole focus of interest is equatorial waves, the linear PE model should be used and is certainly easier to solve.

Acknowledgment. We thank Nancy Norton for her persistence and fortitude in designing and executing all the numerical calculations discussed in this work and shown in the figures.

APPENDIX A

The Long-Wave Limit

a. The gBE model

A single equation for v can be formed for the gBE by eliminating Φ from equations (17) and (20). It is

$$gBE \qquad MNv + k^2Kv = 0, \tag{A1}$$

where

$$M = (c - y^2)\frac{d^2}{dy^2} + 2y\frac{d}{dy} - 2, \tag{A2}$$

$$N = \frac{d^2}{dy^2} - (c^{-1} + y^2), \tag{A3}$$

and K is a complicated fourth order operator in y. In the long wave limit, with k^2 equal zero but c finite, the governing equation for the PE is

$$PE \qquad Nv = 0. \tag{A4}$$

The gBE boundary conditions in an infinite domain, Eq. (28), are those of the PE, so that the PE Rossby and Kelvin wave solutions given in Eqs. (38) and (39), which satisfy Eq. (A4), are also solutions of the gBE. In a bounded domain, the Choice 2 boundary conditions for the gBE, Eq. (27) with k^2 set to zero, are those of the PE with no condition on χ at the boundaries. Thus the PE solutions are again solutions of the gBE. For Choice 1 boundary conditions, however, χ_y is set to zero at the boundaries [see Eq. 26]. For the antisymmetric PE modes, the solution to equation (19) with $k^2 = 0$, can be written as

$$\chi = \int_0^y dy' \int_L^{y'} \Phi dy'', \tag{A5}$$

satisfying the χ boundary conditions, so that the antisymmetric PE modes are solutions for Choice 1

boundary conditions. For symmetric modes, however, satisfying the two $\chi_y = 0$ boundary conditions requires

$$\int_L^0 \Phi dy' = 0, \tag{A6}$$

and this is not true for the PE modes. When k^2 is zero, the symmetric homogeneous solution of Eq. (19) for χ is a constant, which does not help in satisfying boundary conditions on χ_y. Thus the PE symmetric modes are not solutions of the gBE when k^2 is zero. When k^2 is non-zero, the symmetric homogeneous χ solution to (19) is $\cosh ky$ which can be used to satisfy χ_y conditions on the boundaries, which is why the χ solution is purely diagnostic for the gBE when $k^2 \neq 0$.

However, symmetric modes for the gBE with choice 1 boundary conditions do exist in the long wave limit, but they satisfy the equation

$$Nv = y, \tag{A7}$$

which is a solution of (A1) when $k^2 = 0$. The eigenvalues and eigenfunctions are not those of the PE, and the latter have a boundary layer structure near the boundaries $y = \pm L$. However, there are the same number of eigensolutions as PE symmetric modes and, for each pair of the infinite set of eigenvalues with $-1 < c < 0$, there is a gBE antisymmetric eigenvalue between them. The first four eigenvalues of this sequence for $L = 5$ are $c \approx -0.759, -0.182, -0.1035, -0.072$, whereas the antisymmetric eigenvalues are $\approx -(2m+1)^{-1}$ for even m. All the eigenvalues have now been discussed because none were found with Nv equal to the symmetric in y, homogeneous solution of the operator M, which is $c + y^2$, for both choices of boundary conditions, and none satisfying Eq. (A7) with Choice 2 boundary conditions.

We have analyzed all the gBE modes in a finite basin with $L = 5$, i.e., those shown in Fig. 8, for k^2 equal to 10^{-3} and 10^{-4}. The modes are the same for both choices of boundary conditions because $k^2 \neq 0$. The conclusion is that all antisymmetric modes, i.e., the even numbered Rossby waves and the low frequency component of the mixed Rossby gravity wave, have

$$\left.\begin{aligned} Nv = O(k^2), \quad \text{hence} \quad MNv = O(k^2) \\ Kv = O(1) \quad \text{as} \quad k^2 \to 0 \end{aligned}\right\}. \tag{A8}$$

Thus the eigenvalues and eigenfunctions are those of the PE as $k^2 \to 0$. However, all symmetric modes, i.e., the odd numbered Rossby, the Kelvin and anti-Kelvin waves, have

$$\left.\begin{aligned} Nv = y + O(k^2), \quad \text{hence} \quad MNv = O(k^2) \\ Kv = O(1) \quad \text{as} \quad k^2 \to 0 \end{aligned}\right\}. \tag{A9}$$

For small k^2, the eigenfunctions have characteristics of both the eigenfunctions for symmetric modes when $k^2 = 0$. Throughout most of the domain the eigenfunctions look like those of the PE, but they have a weak boundary layer structure near $y = L$. The eigenvalue for the first Rossby wave as $k^2 \to 0$ is $c \approx -0.344$, which is between the two eigenvalues of the $k^2 = 0$ modes, but much closer to the PE value of $-1/3$.

Thus, in a bounded domain, the only $k^2 = 0$, antisymmetric modes are those of the PE and this limit is approached regularly by the $k^2 \neq 0$ solutions. However, there are two different, $k^2 = 0$ symmetric modes, and this limit has a discontinuous c singularity for these modes with the eigenfunctions having characteristics of both the $k^2 = 0$ eigenfunctions.

Similar analysis for very small values of k^2 on an infinite β-plane has not been done because of the extremely large number of basis functions needed. With $M = 640$ or 641 in Eq. (29), our results are not accurate for $k^2 < 0.01$. Consistent with the results for increasing values of L (see Figs. 9 and 10), is the interpretation that the infinite domain curves have an infinite slope singularity as $k^2 \to 0$. The infinite gradient of dc/dk^2 implies by Eq. (40) that the modes are dispersive in this limit. This interpretation is supported by the fact that a regular perturbation expansion in k^2 about the $k^2 = 0$ Rossby and Kelvin wave solutions (38) and (39) fails. The order k^2 terms in (17) and (20) force a perturbation v solution that tends to a constant as $|y| \to \infty$ because a series representation as in Eq. (29) has $v_m = O(m^{-1/4})$ as $m \to \infty$. The v solution forced by the eigenvalue perturbation has a series such that $v_m = O(m^{-3/4})$ as $m \to \infty$ or $v \to O(y^{-1})$ as $|y| \to \infty$. The two solutions cannot balance in an infinite domain, so that the expansion fails.

b. *The BE model*

There is similar behavior in the BE in the long wave limit. For both choices of boundary conditions in a finite domain, antisymmetric or even numbered Rossby modes tend to the PE solutions regularly as $k^2 \to 0$. The symmetric or odd numbered Rossby modes do not, and satisfy the equation

$$Nv = y + \gamma y^3 + O(k^2), \tag{A10}$$

where γ is a constant, which has different values for the two choices of boundary conditions. This is consistent with the limiting values of the eigenvalues being different for the different boundary conditions, see Fig. 4. The eigenfunctions for these modes are not like those of the PE. The BE has no Kelvin wave, but the low frequency component of the mixed Rossby–gravity wave and the anti-Kelvin wave with Choice 2 boundary conditions are regular as $k^2 \to 0$. With Choice 2 boundary conditions, the high frequency

component of the mixed Rossby–gravity curve also goes into the origin, but $c \approx -15.7$ for $L = 5$ and $k^2 = 10^{-3}$ and the eigenfunction bears very little resemblance to the PE mixed Rossby–gravity wave with $k = 0$ and $\omega = 1$.

The Rossby wave curves on an infinite β-plane are again best thought of as the limit of those for increasing L. Thus, the symmetric modes are non-dispersive in the long-wave limit, but have a discontinuous c singularity with c tending to the limit of the next gravest antisymmetric mode. The antisymmetric modes have an infinite slope singularity as $k^2 \to 0$, with the infinite slope of dc/dk^2 implying that they are dispersive. This interpretation is again supported by the failure of a regular perturbation expansion in k^2 about $k^2 = 0$ for the BE Rossby waves.

APPENDIX B

The Recursion Relations on an Infinite Equatorial β-Plane

The BE recursion relation (31) is:

$$\begin{aligned} BE\quad & v_{m-4}[m(m-1)(m-2)(m-3)]^{1/2}(c^{-1}-1)E(m-1)[4A(m-1)]^{-1} \\ & + \tfrac{1}{2}v_{m-2}[m(m-1)]^{1/2}[(c^{-1}-1)B(m-1)A(m-1) + (m+1)(c^{-1}+1)E(m+1)/2A(m+1) - 1] \\ & + v_m[m(c^{-1}-1)D(m-1)/2A(m-1) + (m+1)(c^{-1}+1)B(m+1)/2A(m+1) + k^2 + c^{-1} + m + \tfrac{1}{2}] \\ & + \tfrac{1}{2}v_{m+2}[(m+1)(m+2)]^{1/2}[(c^{-1}+1)D(m+1)A(m+1) + m(c^{-1}-1)F(m-1)/2A(m-1) - 1] \\ & + v_{m+4}[(m+1)(m+2)(m+3)(m+4)]^{1/2}(c^{-1}+1)F(m+1)[4A(m+1)]^{-1} = 0, \end{aligned} \tag{B1}$$

where

$$A(m) = (2m+1+k^2)(m+\tfrac{1}{2}+k^2) - (m+\tfrac{1}{2})c + m(c^{-1}+1)(2m-3+k^2-c)[2(c^{-1}-1)]^{-1} + (m+1)(c^{-1}-1)(2m+5+k^2-c)[2(c^{-1}+1)]^{-1}, \tag{B2}$$

$$B(m) = \tfrac{1}{2}(m-1)(1+c) - (1-c)(m+\tfrac{1}{2}+k^2) + (m+1)(2m+5+k^2-c)[2(c^{-1}+1)]^{-1} - (2m-3+k^2-c)(m-\tfrac{1}{2}+k^2+c^{-1})(c^{-1}-1)^{-1}, \tag{B3}$$

$$D(m) = \tfrac{1}{2}(m+2)(1-c) - (1+c)(m+\tfrac{1}{2}+k^2) + m(2m-3+k^2-c)[2(c^{-1}-1)]^{-1} - (2m+5+k^2-c)(m+\tfrac{3}{2}+k^2+c^{-1})(c^{-1}+1)^{-1}, \tag{B4}$$

$$E(m) = 1 - c + (2m-3+k^2-c)(c^{-1}-1)^{-1}, \tag{B5}$$

$$F(m) = 1 + c + (2m+5+k^2-c)(c^{-1}+1)^{-1}. \tag{B6}$$

The gBE recursion relation (32) is:

$$\begin{aligned} gBE\quad & \tfrac{1}{2}v_{m-2}[m(m-1)]^{1/2}(2m-3+k^2+c^{-1})(2m+3+k^2-c) \\ & + v_m[m(1-c^2)(2m+3+k^2-c)(2c)^{-1} + (m+1)(1-c^2)(2m-1+k^2-c)(2c)^{-1} \\ & - (2m+3+k^2-c)(2m-1+k^2-c)(k^2+c^{-1}+m+\tfrac{1}{2})] \\ & + \tfrac{1}{2}v_{m+2}[(m+1)(m+2)]^{1/2}(2m+5+k^2+c^{-1})(2m-1+k^2-c) = 0. \end{aligned} \tag{B7}$$

The diagnostic relations for Φ_m are

$$BE\quad A(m)\Phi_m = v_{m-3}[m(m-1)(m-2)/8]^{1/2}E(m) + v_{m-1}B(m)\left(\frac{m}{2}\right)^{1/2} + v_{m+1}D(m)\left(\frac{m+1}{2}\right)^{1/2} + v_{m+3}[(m+1)(m+2)(m+3)/8]^{1/2}F(m), \tag{B8}$$

$$gBE\quad [c-k^2-2m-1]\Phi_m = v_{m-1}(1-c)\left(\frac{m}{2}\right)^{1/2} + v_{m+1}(1+c)\left(\frac{m+1}{2}\right)^{1/2}. \tag{B9}$$

REFERENCES

Cane, M. A., and E. S. Sarachik, 1979: Forced baroclinic ocean motions. III: The linear equatorial basin case. *J. Mar. Res.*, **37,** 355–398.

Gent, P. R., and J. C. McWilliams, 1982: Intermediate model solutions to the Lorenz equations: Strange attractors and other phenomena. *J. Atmos. Sci.*, **39,** 3–13.

——, and ——, 1983a: Consistent balanced models in bounded and periodic domains. *Dyn. Atmos. Oceans,* **7,** 67–93.

——, and ——, 1983b: Regimes of validity for balanced models. *Dyn. Atmos. Oceans,* **7,** 167.

Holton, J. R., 1969: A note on the scale analyses of tropical motions. *J. Atmos. Sci.*, **26,** 770–771.

Lindzen, R. S., 1966: On the theory of the diurnal tide. *Mon. Wea. Rev.*, **94,** 295–301.

Longuet-Higgins, M. S., 1968: The eigenfunctions of Laplace's tidal equations over a sphere. *Phil. Trans. Roy. Soc. London,* **A262,** 511–607.

McWilliams, J. C., and P. R. Gent, 1980: Intermediate models of planetary circulations in the atmosphere and ocean. *J. Atmos. Sci.*, **37,** 1657–1678.

Matsuno, T., 1966: Quasigeostrophic motions in the equatorial area. *J. Meteor. Soc. Japan,* **44,** 25–43.

Moore, D. W., and S. G. H. Philander, 1977: Modeling of the tropical ocean circulation. *The Sea,* Vol. 6, Interscience, 319–361.

Moura, A. D., 1976: The eigensolutions of the linearized balance equations over a sphere. *J. Atmos. Sci.*, **33,** 877–907.

Simmons, A. J., B. J. Hoskins and D. M. Burridge, 1978: Stability of the semi-implicit method of time integration. *Mon. Wea. Rev.*, **106,** 405–412.